

Transverse Rapidity Dependence of the Proton-Antiproton Ratio as a Signature of the QCD Critical Endpoint

M. Asakawa,¹ S. A. Bass,² B. Müller,² and C. Nonaka³

¹*Department of Physics, Osaka University, Toyonaka 560-0043, Japan*

²*Department of Physics, Duke University, Durham, NC 27708, USA*

³*Department of Physics, Nagoya University, Nagoya 464-8602, Japan*

(Dated: May 21, 2019)

The presence of a critical endpoint in the QCD phase diagram can deform the trajectories describing the evolution of the expanding fireball in the $\mu_B - T$ phase diagram. If the average emission time of hadrons is a function of transverse rapidity, as microscopic simulations of the hadronic freeze-out dynamics suggest, the deformation of the hydrodynamic trajectories will change the transverse rapidity (y_T) dependence of the proton-antiproton ratio when the fireball passes in the vicinity of the critical endpoint. An unusual y_T -dependence of the \bar{p}/p ratio in a narrow beam energy window would thus signal the presence of the critical endpoint.

Lattice-QCD simulations have established that the transition between the hadronic and quark-gluon plasma phases of quantum chromodynamics (QCD) at vanishing baryon chemical potential μ_B is a crossover transition [1]. There has been much speculation that the crossover transition becomes a true first-order phase transition for larger values of μ_B . Several attempts have been made to locate the critical endpoint of the first-order transition line by means of approximate lattice simulations [2, 3, 4]. These results have motivated plans for a systematic exploration of the properties of hot QCD matter as a function of the net baryon density by means of a collision energy scan at the Relativistic Heavy Ion Collider (RHIC) [5]. They are also part of the motivation for building a facility dedicated to the study of compressed baryonic matter at the Facility for Antiproton and Ion Research (FAIR) in Germany. At present, the existence of a critical endpoint associated with the chiral phase transition in QCD has not been established theoretically [6], making an experimental search all the more urgent.

Ideas for experimental signatures for the presence of the critical endpoint have mostly focused on fluctuations in certain observables related to the order parameter of the chiral transition in QCD [7, 8]. General arguments lead one to believe that such fluctuations are enhanced in the vicinity of the critical point. Unfortunately, several reasons throw doubt on the usefulness of fluctuation observables as practical signatures of the critical point. First, fluctuations are suppressed, compared to the static case, when the matter passes rapidly through the critical region during the expansion due to critical slowing down [9]. Secondly, the hot matter does not freeze out at the critical point, but only after substantial additional cooling, when the critical fluctuations may well have been washed out. Finally, it is unclear in which observable fluctuations are most promising experimentally. In exploratory experiments at the CERN-SPS, only fluctuations in the K/π ratio at beam energies below 40 GeV/A have shown signs of an unusual behavior [10, 11].

Here we propose a possible signature of the presence of a critical endpoint in the QCD phase diagram, which may be more robust than fluctuations associated with the order parameter of the chiral phase transition. Our idea is based on the observation that the critical point serves as an attractor of the hydrodynamical trajectories in the $\mu_B - T$ plane describing the expansion of the hot matter [12]. We describe below how this focusing effect manifests itself in an experimental observable.

The universality argument tells us that the critical exponents around second order phase transitions are determined only by the dimensionality and symmetry of the system. The QCD critical endpoint, if it exists, belongs to the same universality class as the 3-dimensional Ising model and liquid-gas phase transition [8]. The singular part of the thermodynamic variables near the critical point is a function of two variables, which can be mapped onto the variables characterizing the phase diagram of the 3-dimensional Ising model: the reduced temperature $r = (T - T_c)/T_c$ and the external magnetic field h . In the QCD phase diagram, the axis corresponding to r points in the direction of the phase boundary; the direction of the axis associated with the variable h is not known [9, 13]. However, two statements about the critical region can be safely made [9]. First, the region is more elongated along the r -direction, because the critical exponent associated with r is larger than that associated with h . Second, relaxation times corresponding to motion across the phase boundary are dominated by the dynamical critical exponent associated with h , which is much larger than that associated with the variable r .

The focusing effect can now be understood as follows. The entropy density s and the baryon density n_b depend in different ways on r and h . As a result, the ratio s/n_b , which is constant along an isentropic trajectory, assumes many different values in the vicinity of the critical endpoint. Therefore, hydrodynamic trajectories for a range of different values of s/n_b pass near the critical point, thus causing the focusing effect.

The extent of the focusing region depends on the size of the critical region in the $\mu_B - T$ plane, in which thermodynamic susceptibilities are significantly enhanced by the critical exponents. The size of the attractive basin can, in principle, be determined by lattice-QCD simulations. At the moment this information is not available, as the location and even the existence of the critical point in QCD are not established. Model studies in simplified theories suggest that the size of the attractive region is sensitive to calculational details [14]. Here we will simply assume that the critical region is sufficiently large to induce a significant focusing effect. We use the model of Nonaka and Asakawa [12] to describe the influence of the critical endpoint on the thermodynamic variables. In this model the entropy density is obtained by interpolation between the entropy densities s_H, s_Q of the hadronic and quark phase as

$$s(T, \mu_B) = \frac{1}{2} (1 - \tanh S_c) s_H(T, \mu_B) + \frac{1}{2} (1 + \tanh S_c) s_Q(T, \mu_B), \quad (1)$$

where $S_c(T, \mu_B)$ is proportional to the critical part of the entropy density obtained by rescaling the expressions from the 3-dimensional Ising model. The proportionality constant entering into the definition of S_c determines the size of the influence region of the critical endpoint. Here we differ from ref. [12] by choosing the parameters $\Delta T_{\text{crit}} = 20$ MeV, $\Delta \mu_{\text{crit}} = 100$ MeV, $D = 0.5$. This choice yields a much narrower critical region as shown in Fig. 1. The width of the cross-over between the two phases at $\mu_B = 0$ is approximately 45 MeV, in rough agreement with lattice-QCD results [15].

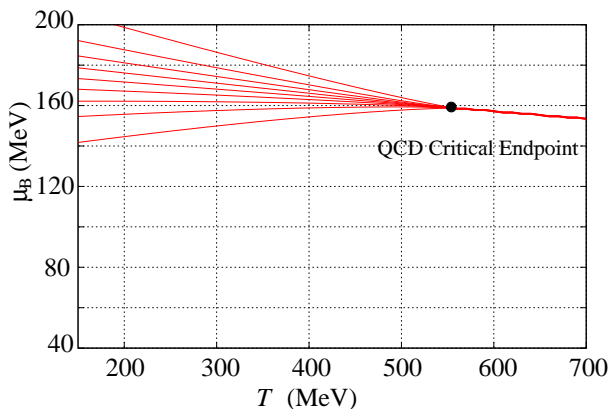


FIG. 1: Critical region in the $\mu_B - T$ plane. The thick solid line to the right of the black dot shows the location of the phase boundary, starting at the critical endpoint $(\mu_c, T_c) = (550, 159)$ MeV. The thin lines to the left indicate the contours of equal values of the cross-over parameter $\tanh S_c$ between -0.8 and $+0.8$ in increments of 0.2 .

The main characteristic of the fireball evolution in the presence of a critical endpoint is that hydrodynamical

trajectories, which would normally tilt to the right after crossing the phase boundary (see solid line in Fig. 2), make a detour into the vicinity of the critical point and then turn to the left as the temperature falls below T_c (see dashed line in Fig. 2). For our argument, the important difference is the behavior just below T_c , where both T and μ_B decrease for trajectories with a critical point, while μ_B stays roughly constant or increases with falling temperature for trajectories without a critical point. This difference can have visible consequences if hadron emission occurs over a finite range of temperatures, and if emission from different points along the trajectory can be discriminated. For instance, the ratio μ_B/T monotonically increases below T_c along the “normal” (solid) trajectory in Fig. 2, implying a falling antiproton-to-proton (\bar{p}/p) ratio. On the other hand, the dashed trajectory in Fig. 2 implies an approximately constant or even slightly decreasing value of μ_B/T and thus a rising \bar{p}/p ratio as the temperature falls below T_c .

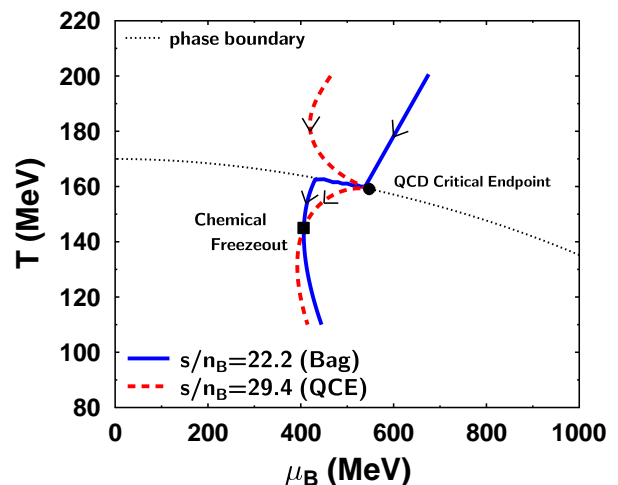


FIG. 2: Hydrodynamical trajectories in the QCD phase diagram with and without the presence of a critical endpoint. The trajectory in the absence of a critical point is shown as solid line in the $\mu_B - T$ plane; the trajectory in the presence of a critical point is shown dashed. The two trajectories meet at the chemical freeze-out point. Arrows indicate the direction of time evolution.

In order to confirm this qualitative argument we present a quantitative analysis based on the assumption that the attractive basin of the critical point is reached in central Pb+Pb collisions at 40 GeV/A. In Fig. 3 we show the \bar{p}/p ratio along the dashed and solid trajectories shown in Fig. 2 as a function of the entropy density between T_c and the chemical freeze-out point, which has been determined to lie at $(\mu_{\text{ch}}, T_{\text{ch}}) \approx (400, 145)$ MeV by a statistical model fit to experimental data [20]. As anticipated, the \bar{p}/p ratio falls between the phase boundary and chemical freeze-out for the “normal” trajectory, but rises for the trajectory deformed by the presence of the critical endpoint.

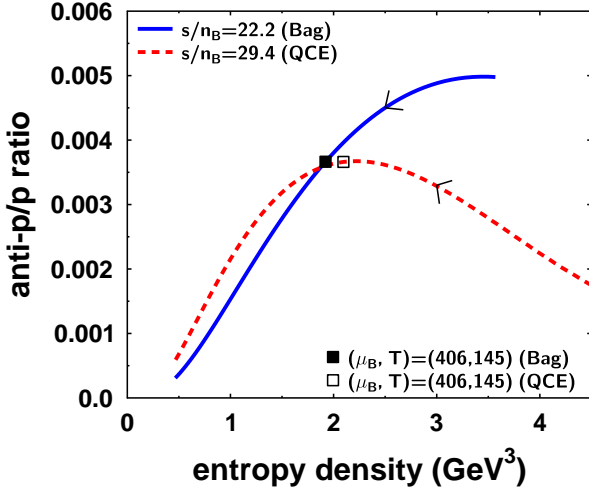


FIG. 3: Antiproton-to-proton ratio along the dashed and solid trajectories shown in Fig. 2 as a function of the entropy density. The curves start at the phase boundary $T_c \approx 160$ MeV and continue down to $T \approx 110$ MeV. The location of the chemical freeze-out point (μ_{ch}, T_{ch}) deduced from experimental data is indicated by the open and solid squares. Note that the \bar{p}/p ratio falls between the phase boundary and chemical freeze-out for the “normal” trajectory and rises for the trajectory deformed by the critical endpoint.

We next discuss how baryon emission from different points along the hydrodynamical trajectory may be distinguished. We first note that data from Au+Au collisions at RHIC have been explained by the assumption that the emission of hadrons with intermediate transverse momentum ($p_T \sim 2 - 5$ GeV/c) occurs at the phase boundary by recombination of constituent quarks [16, 17]. Bulk freeze-out of hadrons, on the other hand, occurs when the mean free path of hadrons becomes comparable to the size of the fireball. The mean free path relevant to transport properties generally grows with increasing hadron momentum. This implies that hadrons with large transverse momentum should freeze out earlier, on average, than hadrons with a small transverse momentum. In the extreme, intermediate p_T hadrons may be produced at or near the phase boundary. This effect can also be understood by invoking detailed balance. A highly energetic hadron, impinging onto the fireball from the outside, would penetrate deeper into the matter than a low-energy hadron. Conversely, energetic hadrons will be emitted, on average from deeper inside the matter and thus earlier than low-energy hadrons.

The differential emission of baryons as a function of transverse momentum can be analyzed quantitatively in the framework of a microscopic hadron transport model, e. g. UrQMD [18, 19]. Such transport models based on relativistic Boltzmann dynamics involving binary hadronic reactions are commonly used to describe the freeze-out and break-up of the fireball produced in

relativistic heavy-ion collisions into hadrons. Utilizing the UrQMD model, we have calculated central Au+Au collisions at a fixed target energy of 40 GeV/A, which may lead to conditions for which the matter passes near the QCD critical point. We then determined the last time of interaction in the medium (“emission time”) for all final-state (anti-)protons. In order to discriminate between “slow” and “fast” hadrons, we choose the transverse rapidity variable $y_T = \frac{1}{2} \ln[(E_T + p_T)(E_T - p_T)]$, which can be considered as the relativistic generalization of the transverse velocity, but is less susceptible to effects caused by resonance decays of excited baryons.

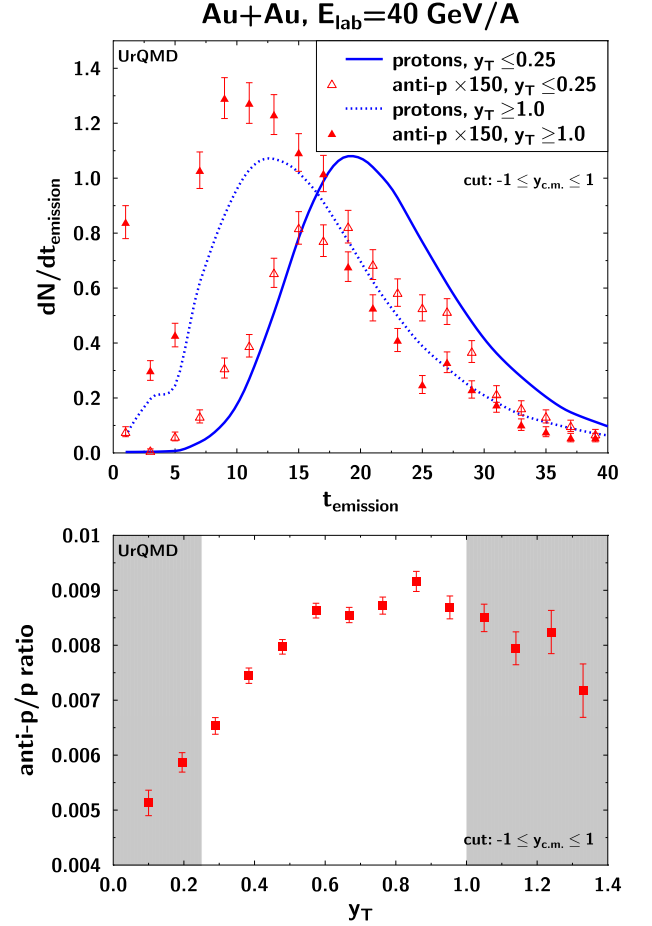


FIG. 4: Top: UrQMD predictions for the emission time (last interaction time) distribution of protons and antiprotons in central Au+Au collisions at 40 GeV/A. The emission time distributions are shown separately for the kinematic windows $y_T < 0.25$ and $y_T > 1$. Fast particles are emitted on average significantly earlier than slow particles. Bottom: \bar{p}/p ratio as a function of transverse rapidity y_T .

The distribution of emission times (counting from the moment of full overlap of the colliding nuclei) for *fast* (anti-)protons with $y_T > 1$ is shown in the top frame of Fig. 4 in comparison with the emission time distribution for *slow* (anti-)protons with $y_T < 0.25$. It is clearly

seen that the emission of protons and antiprotons in the $y_T > 1$ window is correlated with early emission times and occurs approximately 5 fm/c earlier than for slow (anti-)protons. The average emission times for fast protons and antiprotons are 17.6 ± 0.02 and 15.1 ± 0.2 fm/c, respectively, compared to 22.9 ± 0.02 and 21.2 ± 0.2 fm/c for slow moving protons and antiprotons.

The bottom frame of Fig. 4 confirms the expectation from the solid line in Fig. 3, that the \bar{p}/p ratio should rise as a function of y_T in the absence of a critical endpoint. Because the UrQMD calculation does not include finite-density corrections to the antiproton annihilation cross section, the overall value of the ratio should not be compared with experiment. We also note that UrQMD does not contain any physics related to the QCD phase transition and only serves here as a model to study the correlation between emission time and transverse rapidity. We expect the observed correlation to persist in the presence of a critical endpoint.

A search of existing data revealed that the \bar{p}/p ratio in Pb+Pb collisions at the CERN-SPS has been measured as a function of beam energy by the NA49 collaboration, which has published proton and antiproton spectra for fixed-target beam energies of 20, 30, 40, 80, and 158 GeV/A [21]. Interestingly, the antiproton spectrum measured at 40 GeV/A exhibits an anomaly. Whereas the exponential slope of the antiproton spectrum is flatter than the slope of the proton spectrum at other beam energies, it is slightly steeper at 40 GeV/A. A flatter antiproton spectrum is compatible with differential chemical freeze-out on a trajectory similar to the solid trajectory shown in Fig. 2, while a steeper spectrum would require a trajectory of the type expected in the vicinity of the critical point (similar to the solid line in Fig. 2). The relative suppression of antiprotons at large transverse momentum is clearly visible in the spectrum itself (see Fig. 3 in ref. [21]). The size of the statistical errors of the measurement does not permit a firm conclusion about this anomaly, but it is certainly compatible with the arguments presented here.

In summary, we have shown that the evolution of the \bar{p}/p ratio along isentropic curves between the phase boundary in the QCD phase diagram and the chemical freeze-out point is strongly dependent on the presence or absence of a critical endpoint. When a critical point exists, the isentropic trajectory approximately corresponding to hydrodynamical expansion is deformed, and the \bar{p}/p ratio grows during the approach to chemical freeze-out. If nucleons of high transverse momentum are chemically frozen out earlier than the slow nucleons, as it is suggested by microscopic simulations of hadronic dynamics, this result will translate into a \bar{p}/p ratio that falls with increasing transverse momentum instead of a rise in the scenario without critical endpoint. This behavior would only occur at those beam energies, for which the

fireball reaches the critical endpoint.

Note that the location of the critical endpoint in our model study was chosen such that it influences a hydrodynamics trajectory for the conditions reached at a beam energy of 40 GeV/A. For a different location of the critical endpoint, similar behavior would occur at other beam energies. Finally, depending on the actual size of the attractive region around the critical endpoint, the search for an anomaly in the y_T dependence of the \bar{p}/p ratio may require small beam energy steps.

Acknowledgments: This work was supported in part by the U. S. Department of Energy (grant DE-FG02-05ER41367), the Japanese Ministry of Education (grants-in-aid 17540255 and 19740136), and the Mitsubishi Foundation. We also gratefully acknowledge the hospitality and support of the Yukawa Institute for Theoretical Physics and its members, especially K. Fukushima and T. Kunihiro, during its international workshop program entitled *New Frontiers in QCD 2008*. Finally, we thank G. Odyniec for asking the question which inspired this investigation.

-
- [1] Y. Aoki, G. Endrodi, Z. Fodor, S. D. Katz, and K. K. Szabo, *Nature* **443**, 675 (2006).
 - [2] Z. Fodor, S. D. Katz, and K. K. Szabo, *Phys. Lett.* **B568**, 73 (2003).
 - [3] Z. Fodor and S. D. Katz, *JHEP* **04**, 050 (2004).
 - [4] R. V. Gavai and S. Gupta, *Phys. Rev.* **D71**, 114014 (2005).
 - [5] G. S. F. Stephans, *J. Phys.* **G32**, S447 (2006).
 - [6] P. de Forcrand, S. Kim, and O. Philipsen, *PoS LAT2007*, 178 (2007).
 - [7] M. A. Stephanov, K. Rajagopal, and E. V. Shuryak, *Phys. Rev. Lett.* **81**, 4816 (1998).
 - [8] M. A. Stephanov, K. Rajagopal, and E. V. Shuryak, *Phys. Rev.* **D60**, 114028 (1999).
 - [9] B. Berdnikov and K. Rajagopal, *Phys. Rev.* **D61**, 105017 (2000).
 - [10] NA49, C. Roland, *J. Phys.* **G31**, S1075 (2005).
 - [11] NA49, C. Roland, *PoS CERN2006*, 012 (2006).
 - [12] C. Nonaka and M. Asakawa, *Phys. Rev.* **C71**, 044904 (2005).
 - [13] Y. Hatta and T. Ikeda, *Phys. Rev.* **D67**, 014028 (2003).
 - [14] B.-J. Schaefer and J. Wambach, *Phys. Rev.* **D75**, 085015 (2007).
 - [15] Y. Aoki, Z. Fodor, S. D. Katz and K. K. Szabo, *Phys. Lett. B* **643**, 46 (2006).
 - [16] R. J. Fries, B. Müller, C. Nonaka and S. A. Bass, *Phys. Rev. Lett.* **90**, 202303 (2003).
 - [17] V. Greco, C. M. Ko and P. Levai, *Phys. Rev. Lett.* **90**, 202302 (2003).
 - [18] S. A. Bass *et al.*, *Prog. Part. Nucl. Phys.* **41**, 255 (1998).
 - [19] M. Bleicher *et al.*, *J. Phys. G* **25**, 1859 (1999).
 - [20] P. Braun-Munzinger, K. Redlich, and J. Stachel, *nucl-th/0304013*.
 - [21] NA49, B. Lungwitz *et al.*, arXiv:0709.1646 [nucl-ex].